*J. Fluid Mech.* (2012), *vol.* 703, *pp.* 363–373. © Cambridge University Press 2012 
doi:10.1017/jfm.2012.225

# Transverse instability and low-frequency flapping in incompressible separated boundary layer flows: an experimental study

**Pierre-Yves Passaggia, Thomas Leweke† and Uwe Ehrenstein**

IRPHE, UMR 7342 CNRS, Aix–Marseille Université, F-13384 Marseille CEDEX 13, France

(Received 10 January 2012; revised 22 March 2012; accepted 9 May 2012;
first published online 13 June 2012)

The unstable dynamics of a transitional laminar separation bubble behind a two-dimensional bump geometry is investigated experimentally using dye visualizations and particle image velocimetry measurements. For Reynolds numbers above a critical value, the initially two-dimensional recirculation bubble is subject to modulations in the spanwise direction which can trigger vortex shedding. Increasing the Reynolds number further, the unstable behaviour is dominated by a low-frequency flapping motion, well known in transonic flows, and here investigated for the first time experimentally in an incompressible flow regime. These phenomena are characterized by non-intrusive measurements of the spatial structure and the frequencies of the unsteady motion. The results are in excellent agreement with previous numerical and theoretical predictions for the same geometry.

**Key words:** boundary layer separation, instability

## 1. Introduction

Flow separation is a common feature in wall-bounded flows, where it is generally induced by an adverse pressure gradient, which may be due to the presence of a geometrical device, for example. The resulting recirculation bubbles represent sources of instability phenomena, which are often associated with a loss of aerodynamic performance. The review of separated boundary layer flows by Dovgal, Kozlov & Michalke (1994) addresses the well-known convective Kelvin–Helmholtz instability, which has been the object of various numerical (e.g. Pauley, Moin & Reynolds 1990; Kaiktsis, Karniadakis & Orszag 1996) and experimental investigations (e.g. Cherry, Hiller & Latour 1984; Häggmark, Bakchinov & Alfredsson 2000). In addition to this high-frequency dynamics, Dovgal *et al.* (1994) also mention overall feedback effects in separation bubbles, giving rise to global oscillations on a significantly longer time scale. Such low-frequency oscillations are known as buffeting in transonic flows (Crouch *et al.* 2009, and references therein). Low-frequency unsteadiness has also been found in shock-induced separation (Piponniau *et al.* 2009). Addressing laminar incompressible separation induced by a wall-mounted bump, the numerical investigation by Marquillie & Ehrenstein (2003) showed similar dynamics. Stability analyses of this flow configuration have provided further insight concerning the origin of this two-dimensional flapping (Ehrenstein & Gallaire 2008). For separation along

† Email address for correspondence: thomas.leweke@irphe.univ-mrs.fr

https://doi.org/10.1017/jfm.2012.225 Published online by Cambridge University Press

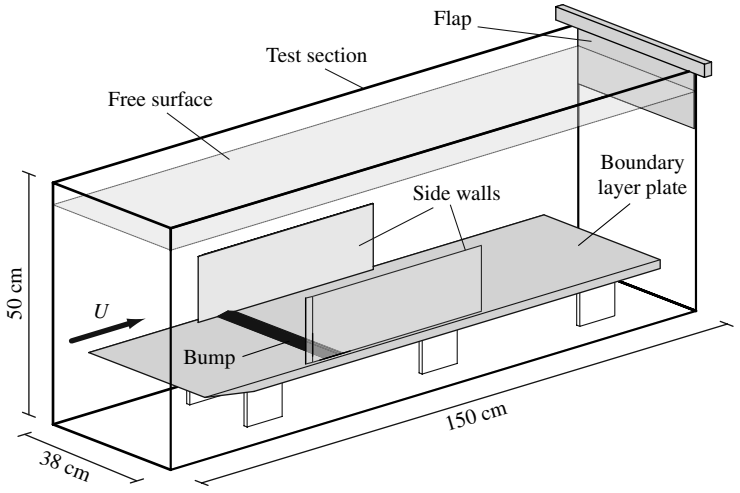



FIGURE 1. Schematic of the experimental set-up. The bump and sidewalls are mobile and can be placed at different downstream positions on the boundary layer plate.

a flat plate induced solely by an adverse pressure gradient, Cherubini, Robinet & De Palma (2010*a*) have found essentially the same behaviour. In addition to the two-dimensional dynamics, separated flows with reattachment were also found to exhibit a slowly growing three-dimensional transverse instability, involving a steady perturbation mode. This was shown numerically for flow over a backward-facing step by Barkley, Gomes & Henderson (2002), and experimentally by Beaudoin *et al.* (2004). Similar observations were made for the boundary layer bump geometry by Gallaire, Marquillie & Ehrenstein (2007) and Cherubini *et al.* (2010*b*). Even though this transverse instability appears first when increasing the Reynolds number, it is eventually dominated by the essentially two-dimensional flapping. Experimental confirmation of this sequence of events, found mainly numerically for an idealized flow case, is still lacking. This is the object of the present paper, in which the same geometry as used initially by Marquillie & Ehrenstein (2003) is considered, and where evidence of both instabilities is presented.

Details about the experimental set-up and measurement techniques are given in § 2. Results concerning the steady recirculation bubbles, transverse instability and the flapping phenomenon are presented in § 3 and discussed in § 4.

## 2. Experimental set-up and parameters

The experimental set-up is shown schematically in figure 1. The flow was investigated in a free-surface low-speed water channel, having a test section with glass walls of dimensions 38 cm (width) × 50 cm (depth) × 150 cm (length). A sharp-leading-edge flat plate, made of Plexiglas and of dimensions 130 cm (length) × 37.5 cm (width) × 2.0 cm (thickness), was mounted in the test section in order to generate a laminar boundary layer. To avoid leading-edge separation, the outflow section had to be partially blocked with a flap. Profiles of the streamwise velocity $u$ as a function of the wall-normal (vertical) coordinate $y$ were measured along the flat plate using particle image velocimetry (PIV): see below. Figure 2(*a*) shows an example of such a measurement, which is extremely close to a Blasius boundary layer

https://doi.org/10.1017/jfm.2012.225 Published online by Cambridge University Press

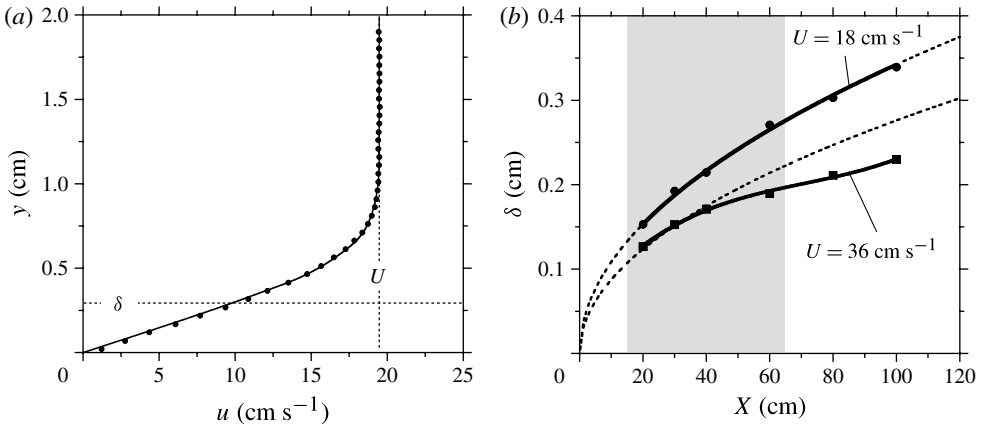



FIGURE 2. Velocity profile above the boundary layer plate without bump. (*a*) Example of $u(y)$ for $U = 18$ cm s$^{-1}$, measured at $X = 80$ cm. The line represents a fit to the Blasius profile without pressure gradient. (*b*) Downstream evolution of the displacement thickness $\delta$ for two values of $U$. The dashed lines represent fits to the theoretical evolution for a Blasius boundary layer (see text), and the shaded area is the interval used for the present study.

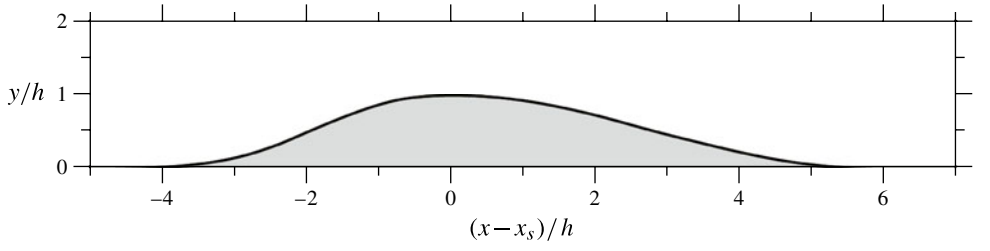



FIGURE 3. Geometry of the boundary layer bump. Two different bump heights were used: $h = 2.2$ mm and $h = 5.5$ mm.

profile, also shown. Such measurements allow the determination of the displacement thickness $\delta$ of the boundary layer, which is one of the parameters characterizing the flow. The evolution of $\delta$ with the downstream distance $X$, measured from the leading edge of the plate, is plotted in figure 2(*b*) for two values of the free-stream velocity $U$. The theoretical expression for the displacement thickness is $\delta(X) = \gamma\sqrt{\nu X/U}$, where $\nu$ is the kinematic viscosity. The proportionality factor $\gamma$ equals 1.721 for a zero-pressure-gradient Blasius boundary layer. The dashed lines in figure 2(*b*) show predictions with slightly different values: $\gamma = 1.453$ and $\gamma = 1.657$ for $U = 18$ cm s$^{-1}$ and $U = 36$ cm s$^{-1}$, respectively. Note that the flap placed at the end of the test section leads to an acceleration of the flow in this region; the boundary layer thickness is therefore slightly decreased there for higher incoming velocities $U$.

Boundary layer separation was induced by placing a smooth bump on the flat plate, whose geometry is shown in figure 3. The same geometry, based on an original design by Bernard *et al.* (2003), was considered in the numerical investigation of Marquillie & Ehrenstein (2003). Two bumps of heights $h = 5.5$ and $h = 2.2$ mm were machined from aluminium alloy. The bumps extended over a spanwise distance of 347 mm and were bounded at each end by additional sidewalls (see figure 1). These walls, of

https://doi.org/10.1017/jfm.2012.225 Published online by Cambridge University Press

dimensions 500 mm × 150 mm × 2 mm, were used to minimize end effects and to generate a well-defined lateral boundary condition. The sharp edges of the sidewalls face the incoming flow and are located at a distance $14h$ upstream of the bump summit.

The problem definition and parameters used here are also the same as in the numerical simulation of Marquillie & Ehrenstein (2003): a reference position is considered (equivalent to the inflow boundary in the simulations), with a corresponding boundary layer displacement thickness $\delta$, which serves as the origin for the downstream coordinate $x$; $y$ and $z$ are the vertical (wall-normal) and transverse (spanwise) coordinates, respectively, and all distances are non-dimensionalized by $\delta$. The bump is then placed in such a way that its summit is located at $x_s = 25\delta$. The non-dimensional parameters governing this flow configuration are the Reynolds number based on the displacement thickness ($Re = U\delta/\nu$), and the relative height of the bump ($h/\delta$). When varying the free-stream velocity of the water channel for a given bump location $X$, both $Re$ and $h/\delta$ evolve simultaneously, since $\delta$ depends on $U$. In the set-up used here, the bump and sidewalls were mobile and could be placed at different positions $X$ along the plate, in order to vary these two parameters independently. In practice, the bump summit was located between $X = 15$ and $X = 65$ cm (illustrated by the shaded area in figure 2*b*), and the free-stream velocity was varied between $U = 6$ cm s$^{-1}$ and $U = 24$ cm s$^{-1}$. This results in the following parameter ranges: $100 < Re < 700$ and $1.6 < h/\delta < 2.1$. In principle, the presence of the bump can modify the displacement thickness evolution depicted in figure 2(*b*), measured without the bump. Therefore, the reference position and corresponding displacement thickness were determined again, in an iterative way using PIV, for each combination of free-stream velocity and bump location considered in this study.

As the flow is extremely sensitive to external disturbances, only non-intrusive measurement techniques were used. Velocity measurements were carried out with PIV (Meunier & Leweke 2003), using an Nd-YAG pulsed laser and an 11 megapixel digital camera. The measurement planes were either parallel to the wall inside the recirculation region, or perpendicular to the wall and aligned with the flow. Time-resolved PIV measurements were performed using a high-speed video camera. In addition, quantitative data was obtained from dye visualizations, in particular concerning the unsteadiness of the separating shear layer, the length of the recirculation zone and the spanwise instability wavelength. Further details are given in the next section.

## 3. Results

### 3.1. *Steady flow*

In the present experiments, the flow was found to be steady for Reynolds numbers below approximately 300 for all bump heights $h/\delta$ considered. The flow is essentially two-dimensional in the central region of the test section, sufficiently far (typically more than 5–7 cm) from the sidewalls. Dye visualizations illustrating this flow regime are presented in figures 4 and 5. The longitudinal cut in figure 4 shows an example of an elongated recirculation zone behind the bump, whereas wall streamline patterns can be seen in figure 5. These were obtained by placing a matrix of dye spots on the wall downstream of the bump and letting streaklines develop for several minutes. The recirculation length $l_c$ can be inferred from such visualizations. The upstream limit of the streaklines marks the separation line of the incoming boundary layer. The reattachment line is given by the location where the initial direction of

https://doi.org/10.1017/jfm.2012.225 Published online by Cambridge University Press

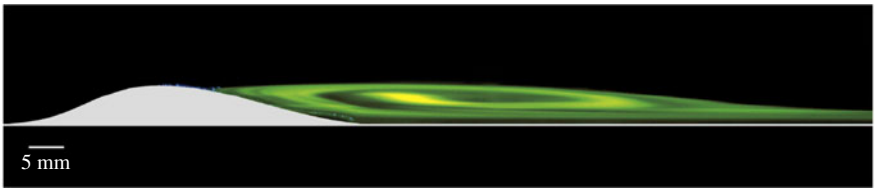



FIGURE 4. Dye visualization of the steady recirculation zone behind the boundary layer bump, for $Re = 174$ and $h/\delta = 1.9$.

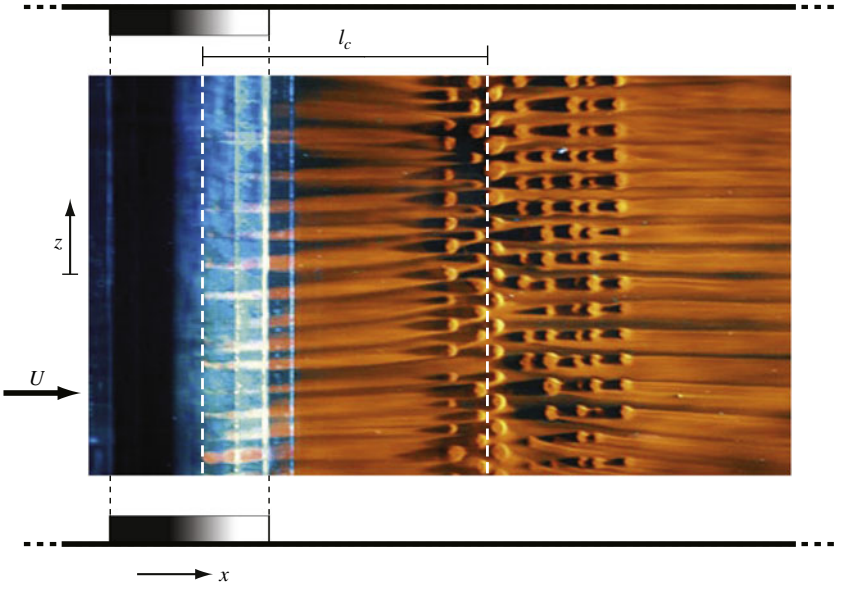



FIGURE 5. Dye visualization of the wall streamline pattern behind the bump for $Re = 244$ and $h/\delta = 1.7$. The dashes represent the separation and reattachment lines.

the streaklines reverses, highlighting the change of sign of $\partial u/\partial y$ at the wall. The variation of the recirculation length with Reynolds number is shown in figure 6 for $h/\delta = 1.7$. This figure also includes results from a two-dimensional direct numerical simulation (DNS), using the algorithm of Marquillie & Ehrenstein (2003) for the same geometry and flow parameters. The experimentally measured recirculation length increases linearly up to $Re \approx 300$, following the numerical results closely. A deviation from this behaviour is observed for higher Reynolds numbers, indicating a transition to a different (three-dimensional) flow regime, discussed in the following section. The same qualitative behaviour was also reported by Sinha, Gupta & Oberai (1981) for the case of separation behind a backward-facing step.

### 3.2. *Transverse instability*

As the Reynolds number is increased beyond 300, the flow becomes three-dimensional. This is illustrated in figure 7, showing a lateral cross-section of the recirculation zone. The dye pattern is modulated in the spanwise direction by a secondary flow,

https://doi.org/10.1017/jfm.2012.225 Published online by Cambridge University Press

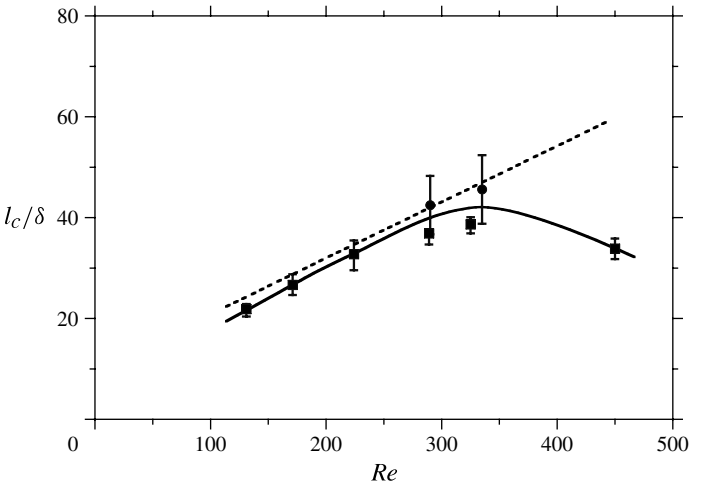



FIGURE 6. Length of the recirculation zone as a function of $Re$, for $h/\delta = 1.7$. Symbols represent experimental measurements: ■, $h = 5.5$ mm; ●, $h = 2.2$ mm. The dashed line results from two-dimensional simulations.

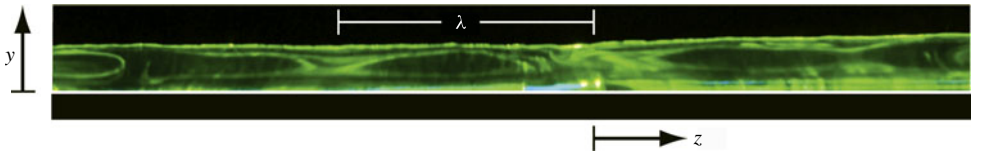



FIGURE 7. Dye visualization of the secondary flow inside the recirculation zone, for $Re = 373$ and $h/\delta = 1.7$. A vertical light sheet is placed $15\delta$ behind the summit and observed from downstream. The vertical coordinate $y$ is here stretched by a factor of 2, in order to show more clearly the structure of the flow.

with a characteristic wavelength λ. No characteristic frequency is associated with the secondary flow; apart from intermittent fluctuations in its amplitude, the instability mode appears to be steady. Further information was obtained by applying proper orthogonal decomposition (POD) (see Sirovich 1987) to a series of 400 velocity fields, measured by PIV at a frequency of 10 Hz in a plane parallel to the wall and inside the recirculation zone. A similar procedure was used by Roy *et al.* (2003). Figure 8(*a*) shows the transverse velocity of the most energetic mode obtained in this analysis. Alternating regions of positive and negative velocity, indicating the presence of counter-rotating streamwise vortices, are located around the reattachment line, and the spanwise wavelength of the three-dimensional instability can again be identified. The value of this wavelength obtained from the two methods in figures 7 and 8(*a*) is $\lambda/\delta = 21 \pm 2$ for $Re \approx 360$ and $h/\delta = 1.7$. This result can be compared to the prediction of the stability analysis carried out by Gallaire *et al.* (2007) for the same geometry. Figure 8(*b*) shows the growth rate of the transverse instability as a function of the spanwise wavelength, obtained in this latter work for $Re = 400$ and $h/\delta = 2$. The maximum growth rate is reached for a wavelength very close to those measured in the present experiments. (The agreement is even better if the wavelength is non-dimensionalized using the respective bump heights $h$.) The growth rates in figure 8(*b*)

https://doi.org/10.1017/jfm.2012.225 Published online by Cambridge University Press

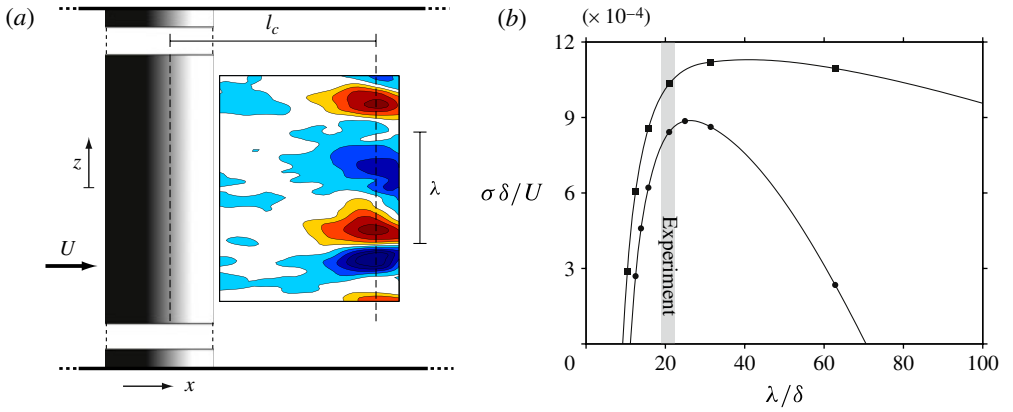



FIGURE 8. (*a*) First POD mode of the transverse velocity $u_z$ in the near-wall region ($y/\delta < 0.3$) of the recirculation zone, revealing the structure of the motion associated with the three-dimensional instability. $Re = 343$ and $h/\delta = 1.7$. Red (blue) contours designate positive (negative) velocities. (*b*) Growth rate $\sigma$ of the three-dimensional instability as a function of the spanwise wavelength, obtained by stability analysis for $h/\delta = 2$. ●, $Re = 400$ (Gallaire *et al.* 2007); ■ $Re = 600$ (present study). The shaded area represents the experimentally observed wavelength range for $Re = 360$ and $h/\delta = 1.7$.

are extremely small; this is consistent with the fact that the spanwise modulations become clearly visible only after a long observation time (of the order of several minutes after the initial start of the flow), as also reported by Beaudoin *et al.* (2004). The regime of spanwise-modulated flow persists up to Reynolds numbers ranging from 500 to 600, depending on $h/\delta$ (see figure 11 below). Whereas for lower Reynolds numbers ($Re \gtrsim 300$) the flow appears to saturate at a steady state, unsteady structures resembling hairpin vortices are shed from the shear layer and amplified downstream near the upper limit in $Re$ of this regime.

### 3.3. *Low-frequency oscillations*

When increasing the Reynolds number further, global oscillations of the recirculation bubble appear. This is illustrated by the visualization sequence in figure 9, obtained after a brief injection of dye into the regions upstream and downstream of the bump. Additional observations along a wall-normal direction showed that these oscillations are essentially two-dimensional in the central region of the flow not affected by end effects. The amplitudes and frequencies of this unsteady motion could be estimated from visualizations such as in figure 9. It was found that, during a certain time interval after injection, the dye tended to concentrate in the shear layer separating from the bump, marking the upper boundary of the recirculation zone. The vertical position of this shear layer could therefore be measured by detecting, in a digital visualization image, the brightest pixel on a vertical line at a given downstream location $x$. The time-dependent position was obtained from analysing each frame of a video sequence, where images were recorded at 25 Hz for ∼1 min. Fast Fourier transforms were then used to calculate the frequency spectra of the shear layer motion. Figure 10(*a*) shows examples of the resulting power spectral density (PSD) distributions, as a function of the non-dimensional frequency $f\delta/U$, and for different Reynolds numbers. For $Re \gtrsim 550$, a peak appears in the spectrum, whose intensity increases with Reynolds

https://doi.org/10.1017/jfm.2012.225 Published online by Cambridge University Press

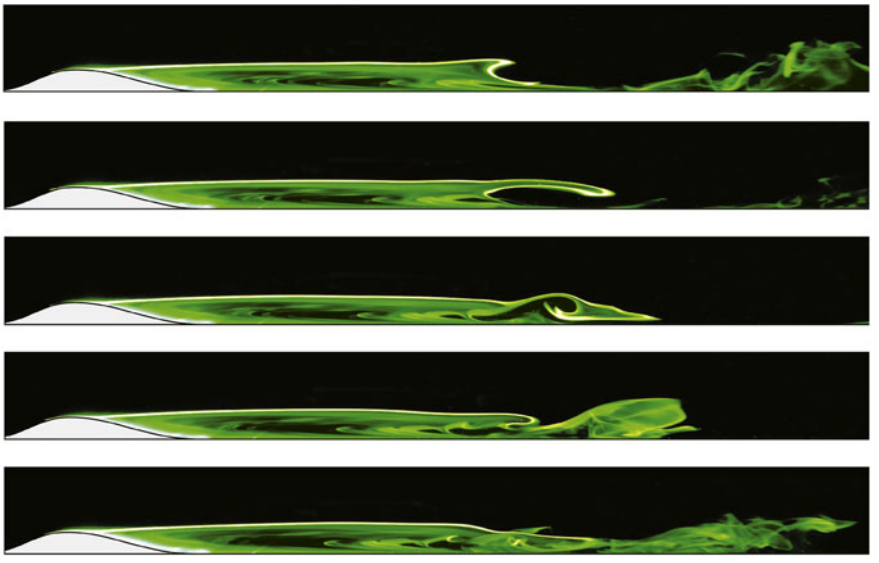


FIGURE 9. Dye visualization sequence (0.25 s between images) of the recirculation zone at $Re = 550$ and $h/\delta = 1.9$.

number. For $Re > 600$, the frequency of the peak is clearly marked, at values around $f\delta/U = 0.007$.

The square of the amplitude of the vertical shear layer displacement, which qualitatively represents the energy of the oscillations, can be estimated by calculating the integral of the PSD over the frequency peak; the result is shown in figure 10(*b*). For $Re \gtrsim 600$, the measured values vary linearly with Reynolds number, indicating that the transition to flapping motion is a supercritical Hopf bifurcation. Extrapolating the linear behaviour to zero amplitude gives an estimate of the critical Reynolds number for this transition; it is here found to be $Re_c \approx 590$. The non-zero amplitudes in the range $500 < Re < 600$ can be explained by the convective amplification, close to the threshold, of residual small-scale fluctuations (background turbulence) in the experiments.

These measurements compare remarkably well with the numerical simulation results of Marquillie & Ehrenstein (2003), who reported a critical Reynolds number in the vicinity of 610 for the onset of global oscillations, with a frequency $f\delta/U = 0.0075$, for a slightly different bump height $h/\delta = 2$. At a higher Reynolds number ($Re = 650$), the spectrum obtained by Marquillie & Ehrenstein (2003) exhibits, in addition to the low-frequency flapping peak, a band of higher frequencies associated with the Kelvin–Helmholtz instability of the shear layer. These frequencies could not be measured from dye visualization sequences here, due to the limited video frame rate. Therefore, time-resolved high-speed PIV measurements of the flow inside the recirculation bubble were carried out. Figure 10(*c*) shows the PSD of the time-dependent wall-normal velocity component, measured a short distance away from the wall ($y/\delta = 1.3$) at a downstream location $x/\delta = 60$. The low-frequency peak is clearly visible, as well as a second group of higher frequencies in the range of values reported by Marquillie & Ehrenstein (2003). The global stability analysis of Ehrenstein & Gallaire (2008) has shown that the non-normal interaction of unstable two-dimensional modes is at the origin of the flapping. Some further computations were carried out

https://doi.org/10.1017/jfm.2012.225 Published online by Cambridge University Press

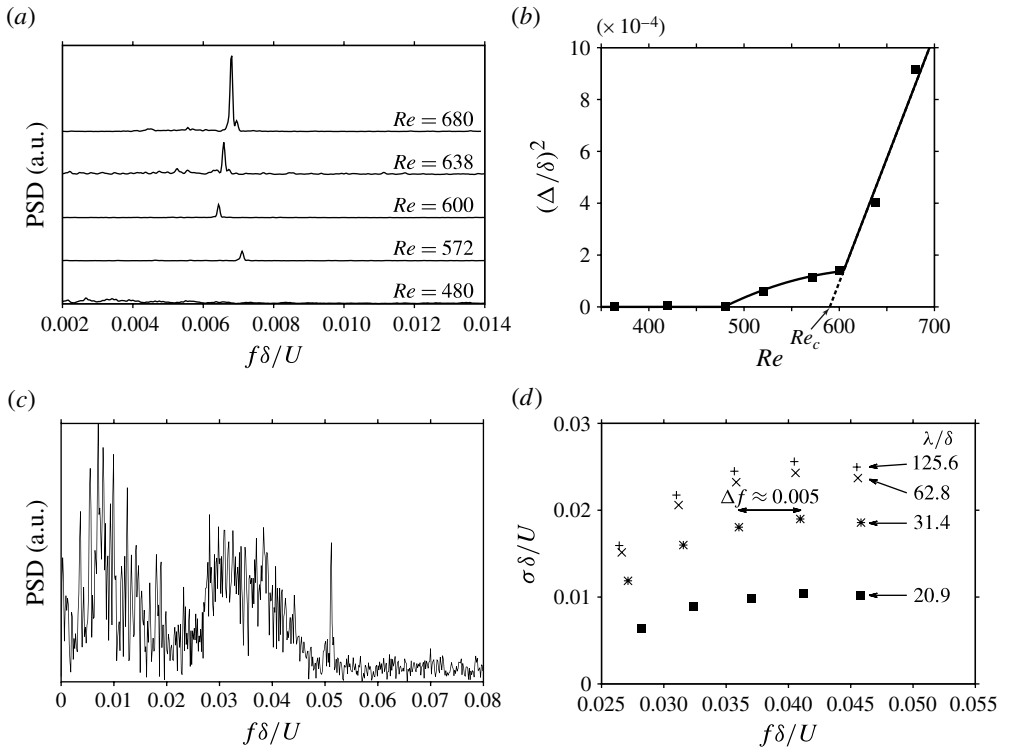



FIGURE 10. (*a*) PSD of the shear layer oscillations at $x/\delta = 35$ and $h/\delta = 1.87 \pm 0.03$, and for various Reynolds numbers. (*b*) Squared normalized amplitude $\Delta/\delta$ of the shear layer displacement measured in (*a*). (*c*) PSD of the shear layer oscillations, obtained from PIV measurements at $x/\delta = 60$. (*d*) Global eigenvalue spectrum of the modes associated with the flapping, computed for $Re = 600$, $h/\delta = 2$ and various spanwise wavelengths $\lambda/\delta$.

at $Re = 600$ to assess the evolution of this instability for finite spanwise wavelengths. The results are depicted in figure 10(*d*). Oscillatory modes are seen to be dominant for large wavelengths with individual frequencies in the Kelvin–Helmholtz range, which is in agreement with the spectrum in figure 10(*c*). As explained in Ehrenstein & Gallaire (2008), their spacing $\Delta f$ is associated with the low flapping frequency. Note that the three-dimensional steady mode is also present at $Re = 600$ (figure 8*b*), but with a much lower amplification rate, its maximum being $\sigma\delta/U = 1.1 \times 10^{-3}$ at $\lambda/\delta \approx 40$.

## 4. Discussion

The different regimes of the flow behind a boundary layer bump are summarized in figure 11 for the range of bump heights $1.6 < h/\delta < 2.1$. The transition between steady flow and transverse instability is seen to occur at an almost constant Reynolds number, whereas the onset of the two-dimensional flapping motion varies with the bump height. At the same time, the low frequency associated with the global flapping is only weakly dependent on the precise parameter values, at least for the moderately supercritical Reynolds numbers considered here.

The flow dynamics observed in the experiment are in excellent agreement with previous numerical results for the same geometry. The linear increase of the recirculation length for steady-state Reynolds numbers, reported in previous

https://doi.org/10.1017/jfm.2012.225 Published online by Cambridge University Press

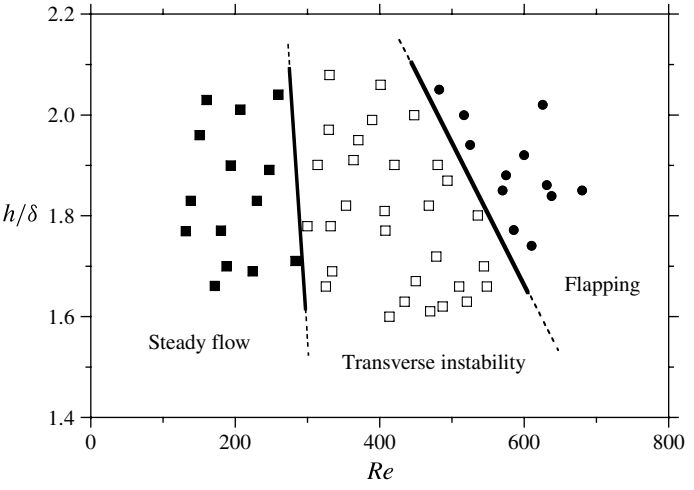



FIGURE 11. Experimental stability diagram for the separated boundary layer flow, as a function of Reynolds number and non-dimensional bump height.

experimental and numerical investigations (Sinha *et al.* 1981; Marquillie & Ehrenstein 2003) is retrieved. For $Re > 300$, steady three-dimensional flow has been observed, with a characteristic spanwise wavelength very close to the theoretical predictions of Gallaire *et al.* (2007). For higher Reynolds numbers ($Re > 500$), rapid oscillations are found, reminiscent of the noise amplifier dynamics due to the Kelvin–Helmholtz instability. At $Re \approx 590$, i.e. very close to the Reynolds number reported by Ehrenstein & Gallaire (2008), a transition occurs to global low-frequency and quasi-two-dimensional oscillations of the recirculation bubble.

Previous investigations referred to an overall growth–decay mechanism in wall-bounded elongated recirculation bubbles (Cherry *et al.* 1984; Dovgal *et al.* 1994). The associated dynamics are known as buffeting in transonic flow regimes, and it has also been documented in shock-induced separation (Crouch *et al.* 2009; Piponniau *et al.* 2009). The present experimental investigation confirms previous numerical studies and provides strong evidence that global low-frequency flapping of a recirculation zone is also inherent to incompressible wall-bounded laminar separated flows.

## Acknowledgement

The authors gratefully acknowledge the financial support from the French *Agence Nationale de la Recherche* (project no. ANR-09-SYSC-001).

## REFERENCES

BARKLEY, D., GOMES, M. G. M. & HENDERSON, R. D. 2002 Three-dimensional instability in flow over a backward-facing step. *J. Fluid Mech.* **473**, 167–190.

BEAUDOIN, J.-F., CADOT, O., AIDER, J.-L. & WESFREID, J. 2004 Three-dimensional stationary flow over a backward facing step. *Eur. J. Mech.* B **23**, 147–155.

BERNARD, A., FOUCAUT, J. M., DUPONT, P. & STANISLAS, M. 2003 Decelerating boundary layer: a new scaling and mixing length model. *AIAA J.* **41**, 248–255.

CHERRY, N. J., HILLER, R. & LATOUR, M. P. 1984 Unsteady measurements in a separating and reattaching flow. *J. Fluid Mech.* **144**, 13–46.

https://doi.org/10.1017/jfm.2012.225 Published online by Cambridge University Press

CHERUBINI, S., ROBINET, J.-C. & DE PALMA, P. 2010*a* The effects of non-normality and nonlinearity of the Navier–Stokes operator on the dynamics of a large laminar separation bubble. *Phys. Fluids* **22**, 014102.

CHERUBINI, S., ROBINET, J.-C., DE PALMA, P. & ALIZARD, F. 2010*b* The onset of three-dimensional centrifugal global modes and their nonlinear development in a recirculating flow over a flat surface. *Phys. Fluids* **22**, 114102.

CROUCH, J. D., GARBARUK, A., MAGIDOV, D. & TRAVIN, A. 2009 Origin of transonic buffet in aerofoils. *J. Fluid Mech.* **628**, 357–369.

DOVGAL, A. V., KOZLOV, V. V. & MICHALKE, M. M. 1994 Laminar boundary layer separation: instability and associated phenomena. *Prog. Aerosp. Sci.* **30**, 61–94.

EHRENSTEIN, U. & GALLAIRE, F. 2008 Two-dimensional global low-frequency oscillations in a separating boundary-layer flow. *J. Fluid Mech.* **614**, 315–327.

GALLAIRE, F., MARQUILLIE, M. & EHRENSTEIN, U. 2007 Three-dimensional transverse instabilities in detached boundary layers. *J. Fluid Mech.* **571**, 221–233.

HÄGGMARK, C. P., BAKCHINOV, A. A. & ALFREDSSON, P. H. 2000 Experiments on a two-dimensional laminar separation bubble. *Phil. Trans. R. Soc. Lond.* A **358**, 3193–3205.

KAIKTSIS, L., KARNIADAKIS, G. E. & ORSZAG, S. A. 1996 Unsteadiness and convective instabilities in two-dimensional flow over a backward-facing step. *J. Fluid Mech.* **321**, 157–187.

MARQUILLIE, M. & EHRENSTEIN, U. 2003 On the onset of nonlinear oscillations in a separating boundary-layer flow. *J. Fluid Mech.* **490**, 169–188.

MEUNIER, P. & LEWEKE, T. 2003 Analysis and treatment of errors due to high velocity gradients in particle image velocimetry. *Exp. Fluids* **35**, 408–421.

PAULEY, L. L, MOIN, P. & REYNOLDS, W. C. 1990 The structure of two-dimensional separation. *J. Fluid Mech.* **220**, 397–411.

PIPONNIAU, S., DUSSAUGE, J.-P., DEBIEVE, J. & DUPONT, P. 2009 A simple model for low-frequency unsteadiness in shock induced separation. *J. Fluid Mech.* **629**, 87–108.

ROY, C., LEWEKE, T., THOMPSON, M. C. & HOURIGAN, K. 2003 Experiments on the elliptic instability in vortex pairs with axial core flow. *J. Fluid Mech.* **677**, 383–416.

SINHA, S. N., GUPTA, A. K. & OBERAI, M. M. 1981 Laminar separating flow over backsteps and cavities. Part 1. Backsteps. *AIAA J.* **19**, 1527–1530.

SIROVICH, L. 1987 Turbulence and the dynamics of coherent structures. *J. Appl. Math.* **45**, 561–590.

https://doi.org/10.1017/jfm.2012.225 Published online by Cambridge University Press